Surface Science 645 (2016) 56–62

Contents lists available at ScienceDirect

Surface Science

journal homepage: www.elsevier.com/locate/susc

Carbon adsorption on tungsten and electronic field emission

Maykel Márquez-Mijares [a,b,c], Bruno Lepetit [b,c], Didier Lemoine [b,c]

[a] Instituto Superior de Tecnologas y Ciencias Aplicadas, Ave. Salvador Allende y Luaces Quinta de Los Molinos, Plaza, La Habana 10600, Cuba
[b] Université de Toulouse, UPS, Laboratoire Collisions Agrégats Réactivité, IRSAMC, F-31062 Toulouse, France
[c] CNRS, UMR5589, France

ARTICLE INFO

Article history:
Received 20 August 2015
Accepted 30 October 2015
Available online 6 November 2015

Keywords:
Electronic field emission
Density functional theory
Adsorption
Carbon
Tungsten

ABSTRACT

Electronic emission taking place at the electrodes of high voltage systems and responsible for detrimental breakdown processes is known to be strongly dependent on the cathode surface state and in particular on the presence of carbon contamination. To understand better the effect of carbon adsorption on cathode electronic emission, density functional theory calculations are reported for bulk bcc tungsten as well as for clean and carbon-covered W(100) surfaces for several coverages up to 2 ML. Adsorption geometries and energies, work functions and electronic densities of states are analyzed to assess the effect of the presence of adlayers on surface electronic field emission properties. It is shown that flat carbon adlayer deposition on clean W(100) surfaces induces an increase of the surface work function and a decrease of electronic density near the Fermi level. Both factors contribute to reducing electronic field emission levels.

1. Introduction

Electronic field emission [1] poses challenges to the design of vacuum insulation structures in high voltage systems [2–4]. One well-known method of reducing the intensity of such field emission current is to raise the pressure in the vacuum system, typically from high or ultrahigh vacuum to pressures on the order of 10^{-4}–10^{-2} Pa [5–9]. This effect has been known for quite some time and has been investigated recently in detail for tungsten carbide cathodes [10,11]. It is known to occur also for tungsten electrodes [12–14]. These changes in field emission intensity as a function of ambient pressure are related to modifications of the cathode surface state at micro- or nano-scales. There is no consensus however on the detailed nature of these surface changes. Some works invoke destruction of emitting nanotips by sputtering [5,8,9] or implantation within dielectric inclusions [15]. Others believe that contamination of the surface may result from adsorption of H_2, CO, N_2, O_2… ambient gases [16,12]. However, in a recent experimental characterization of the cathode state, the main contaminant was found to be carbon [11]. It is thus desirable to investigate the influence of carbon adsorption on the electronic emission properties of metallic surfaces like tungsten.

In particular, we wish to discriminate possible effects arising from the chemical nature of the adsorbate layer from those arising from its morphology. Indeed, a carbon deposit layer may be a regular flat one or on the contrary may consist of nano/micro-tips increasing the roughness of the surface and enhancing electronic emission properties. The focus of the present paper is on the influence on electronic emission properties of the chemical nature of the adsorbate rather than its morphology. Thus, we consider flat adsorbed carbon layers on tungsten substrates. We analyze in more details the changes in work function and density of states near Fermi level resulting from carbon adsorption, since both have a strong influence on emission properties. Calculations are performed using periodic density functional theory (DFT).

The present study has implications beyond the present electronic emission problem. Indeed, tungsten is often used as a substrate on which thin films can be grown. Cleanliness of the surface is a key issue in this field and carbon is known to be the most common contaminant of tungsten substrates [17,18]. Our study provides insight on how substrates are contaminated by such thin carbon layers. More generally, tungsten surfaces are known to be highly reactive with carbon monoxide and hydrocarbons and adsorption of such gases often occurs dissociatively, yielding carbonaceous adlayers on tungsten, akin to the ones considered here [19].

The computational method is presented in Section 2. Sections 3, 4 and 5 report computed properties for the bulk, the clean W(100) surface and the carbon-covered surfaces, respectively. Structural and mechanical properties are presented briefly to assess the accuracy of the calculations, but work functions (W_F), densities of states (DOS) and local densities of states (LDOS) which directly control electronic emission are analyzed in detail. Whenever possible, the accuracy of our results is discussed by comparison with previous calculations and experimental results.

E-mail addresses: mmarquez@instec.cu (M. Márquez-Mijares), bruno.lepetit@irsamc.ups-tlse.fr (B. Lepetit), didier.lemoine@irsamc.ups-tlse.fr (D. Lemoine).

http://dx.doi.org/10.1016/j.susc.2015.10.059
0039-6028/

2. Computational method

The ab initio total-energy and molecular dynamics program VASP (Vienna ab initio simulation program) developed at the Institut für Materialphysik of the Universität Wien has been used for all DFT calculations [20–23]. The electron–ion interaction for all atomic species (W and C) was described by the projector augmented wave potential (PAW) [24,25] optimized for the GW calculations [26–28]. The exchange–correlation energy has been calculated within the generalized gradient approximation (GGA) using the revised form of the Perdew, Burke, and Ernzerhof functional (PBE) [29–31]. We performed convergence tests with different valence bases and eventually chose to treat the 5s, 5p, 6s and 5d tungsten electrons and the 2s and 2p carbon electrons as valence ones. Fractional occupancies were calculated using a second-order Methfessel–Paxton smearing function [32] with a width of 0.2 eV. All plane waves of the basis set were expanded up to a kinetic energy cutoff of 580 eV, ensuring a good convergence of total energies with an accuracy of the order of 5 meV. The tungsten structure we consider here is body-centered cubic (bcc). The optimized lattice parameter has been calculated using the smallest unit cell consisting of one atom and its reciprocal space of k-points was generated automatically with the Monkhorst–Pack method [33] using a grid of $(15 \times 15 \times 15)$ points. This value ensures the same convergence of the total energy as the one obtained with the cutoff value. The W(100) face is modeled using a seven-, nine- or eleven-layer symmetric slab. In all cases more than seven equivalent vacuum layers (>10 Å) were used. Wood's notations [19] are used to define adsorbate coverage: p(2 × 2) is used for 0.25 ML (mono-layer) coverage, c(2 × 2) for 0.5 ML and p(1 × 1) for 1 ML. The reciprocal space for these different coverages was sampled with $(8 \times 8 \times 1)$, $(11 \times 11 \times 1)$ and $(15 \times 15 \times 1)$ k-points grids, respectively. Three types of symmetric adsorption sites are considered. H sites are the hollow ones located above sublayer W atoms, T and B sites are located on top of surface W atoms or above the center between two of them, respectively (see Fig. 1). When we consider a second adsorbate layer, adsorption site labeling remains the same.

3. Bulk results

We first perform bulk property calculations to check the accuracy of our model. Tungsten is known to exist in different allotropic forms among which the most stable is a bcc structure. The fcc structure has a cohesive energy nearly 0.5 eV/atom smaller than the bcc one (see for example Table 2 in ref. [34]). Therefore we focus in the following on the bcc structure. Because we are dealing with a cubic structure, the equilibrium lattice constant a_0 and all elastic stiffness constants can be obtained from fits of the dependence of the lattice total energy with respect to two types of strains only. One is the isotropic expansion of the material; it provides the dependence of the total energy per atom with respect to the lattice parameter a which we fit to a Birch–Murnaghan equation of state [35]:

$$E(a) = E_{\mathrm{coh}} + \frac{9a_0^3 B}{32}\left(\left[\left(\frac{a_0}{a}\right)^2 - 1\right]^3 B' + \left[\left(\frac{a_0}{a}\right)^2 - 1\right]^2 \left[6 - 4\left(\frac{a_0}{a}\right)^2\right]\right) \quad (1)$$

to obtain the lattice parameter at equilibrium a_0, the cohesive energy E_{coh}, the bulk modulus B as well as the other fitting parameter B'. The second strain we consider is an isotropic expansion δ in the plane defined by two of the three lattice vectors arbitrarily labeled 1 and 2, along with a volume preserving contraction along the third lattice vector [36]. The dependence of the total energy on δ has an approximate quadratic form:

$$E(\delta) = E_{\mathrm{coh}} + 3(c_{11} - c_{12})\delta^2 \quad (2)$$

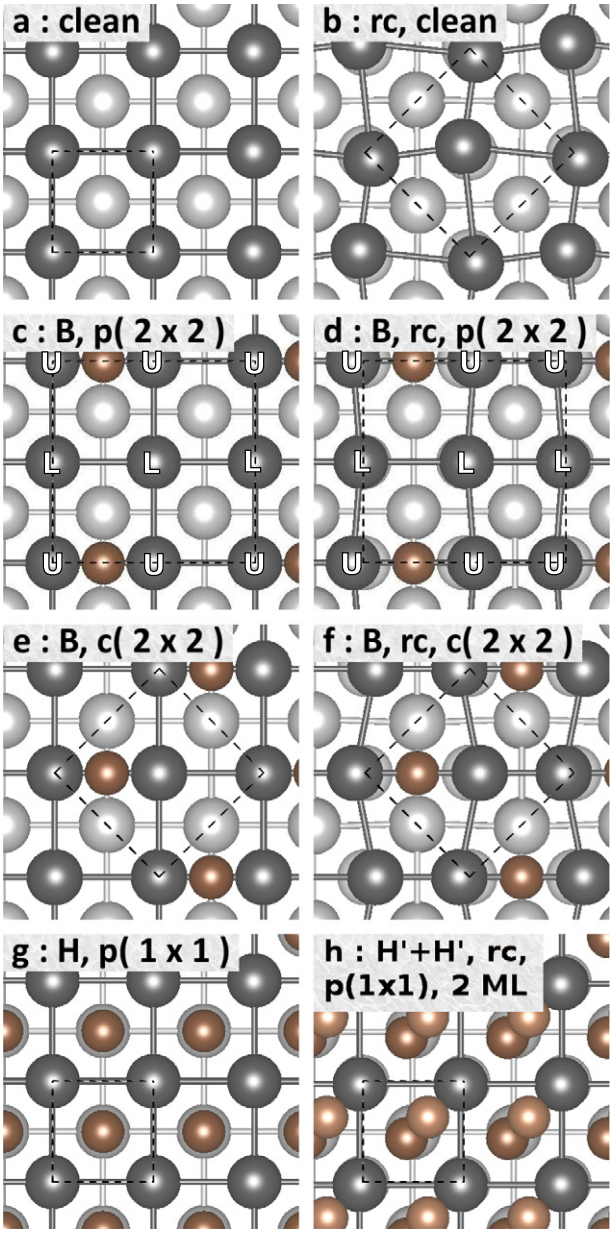

Fig. 1. Examples of adsorption sites and coverages considered in the present work. Large dark gray spheres: surface tungsten atoms. Large light gray spheres: sub-surface tungsten atoms. Small brown spheres: carbon atoms. For the B, p(2 × 2) coverage, the W top layer atoms migrate into two distinct planes and are labeled "U" (upper) and "L" (lower), accordingly. The corresponding heights are given in Table 4. The dashed line encloses the minimum unit cell. In each frame, an inset defines the adsorbing site type (H/B) and the coverage pattern. The right hand side frames correspond to reconstructed surfaces which are indicated by the label "rc". Frame (h) corresponds to a H′ + H′, 2 ML coverage (see text).

where c_{11} and c_{12} are the elastic stiffness constants in the plane of isotropic strain. A parabolic fit of this total energy provides the shear modulus given for the present isotropic cubic structure by: $G = c_{44} = (c_{11} - c_{12})/2$. c_{11} and c_{12} are then obtained separately by: $c_{11} = B + \frac{4}{3}G$ and $c_{12} = B - \frac{2}{3}G$. The results of our calculations are reported in Table 1 for 3 sets of valence electrons and compared with available DFT and experimental results. We don't include in the table the numerous simulation results obtained from semi-empirical potentials, such as those from ref. [34, 37–40] and compiled in ref. [41]. We use the experimental values from ref. [42] (similar to those of ref. [43]) rather than the ones from ref. [44] because the former are extrapolations at 0 K, closer to the calculation conditions, whereas the latter are results in the range of